ADVANCED MATERIALS
www.advmat.de

Quantifying Charge Extraction and Recombination Using the Rise and Decay of the Transient Photovoltage of Perovskite Solar Cells

Lisa Krückemeier, Zhifa Liu, Thomas Kirchartz, and Uwe Rau**

The extraction of photogenerated charge carriers and the generation of a photovoltage belong to the fundamental functionalities of any solar cell. These processes happen not instantaneously but rather come with finite time constants, e.g., a time constant related to the rise of the externally measured open circuit voltage following a short light pulse. Herein, a new method to analyze transient photovoltage measurements at different bias light intensities combining rise and decay times of the photovoltage. The approach uses a linearized version of a system of two coupled differential equations that are solved analytically by determining the eigenvalues of a 2 × 2 matrix. By comparison between the eigenvalues and the measured rise and decay times during a transient photovoltage measurement, the rates of carrier recombination and extraction as a function of bias voltage are determined, and establish a simple link between their ratio and the efficiency losses in the perovskite solar cell.

1. Introduction

The efficiency of halide perovskite solar cells has been continuously rising over the past decade to values above 25%[1–6] that are now approaching the efficiencies of crystalline Si solar cells.[7–9] Future technological development will have to deal with issues of device stability[10,11] but also attempt to further minimize efficiency-limiting loss processes in the bulk and at interfaces within the cell stack.[12–14] The identification and understanding of electrical losses will require to a large degree the ability to characterize solar cells and multilayer stacks with a variety of steady-state,[12,15–18] time-domain[19–27] and frequency-domain techniques[28–32] that are sensitive to the transport and recombination of charge carriers. Especially, time- and frequency-domain techniques offer a large amount of information on dynamic processes in the solar cell,[19,30,33] while posing a substantial challenge in terms of the complexity of data analysis.[19] In case of the often lowly doped or intrinsic halide perovskites,[34] the kinetics of the charge carrier decay in response to a laser pulse in a typical time-domain measurement shows a variety of different features that would have to be numerically simulated in order to accurately extract information from the raw data.[19,35,36] As this can only be done by few and often costly simulation programs and requires time-consuming fitting procedures, a thorough analysis is rarely performed in literature.[37] Thus, work that is primarily aimed at device and process optimization usually analyzes the transients using mono-exponential or bi-exponential fits, while only a minority of method-focused publications delves deeper into the physics of understanding the decays.[26,27,33,38–40]

Here, we show how to use relatively simple analytical solutions to systems of differential equations to extract the key performance-limiting parameters in halide perovskite solar cells from the rise and decay of the transient photovoltage in response to a laser pulse. The results combine the simplicity and comprehensibility of analytical equations with the multiplicity of physical phenomena that occur during a transient experiment on a perovskite solar cell. Transient experiments contain information on phenomena such as recombination and extraction of charge carriers that are difficult to disentangle from each other using traditional approaches.[41] Furthermore, capacitive charging and discharging of electrodes affect the rise and decay times of transients thereby adding complexity to the data analysis.[26,42,43] We solve this problem by creating a numerical model, linearizing it around a bias condition and then solving it analytically by determining the eigenvalues of a 2 × 2 matrix. The model yields two time constants (the negative inverse eigenvalues), one for the rise and one for the decay of the photovoltage after the pulse. These two time

---

L. Krückemeier, Z. Liu, T. Kirchartz, U. Rau
IEK5-Photovoltaik
Forschungszentrum Jülich
52425 Jülich, Germany
E-mail: t.kirchartz@fz-juelich.de; u.rau@fz-juelich.de
L. Krückemeier, U. Rau
Jülich Aachen Research Alliance
JARA-Energy and Faculty of Electrical Engineering and Information Technology
RWTH Aachen University
Schinkelstr. 2, 52062 Aachen, Germany
T. Kirchartz
Faculty of Engineering and CENIDE
University of Duisburg-Essen
Carl-Benz-Str. 199, 47057 Duisburg, Germany

The ORCID identification number(s) for the author(s) of this article can be found under https://doi.org/10.1002/adma.202300872

© 2023 The Authors. Advanced Materials published by Wiley-VCH GmbH. This is an open access article under the terms of the Creative Commons Attribution License, which permits use, distribution and reproduction in any medium, provided the original work is properly cited.

DOI: 10.1002/adma.202300872

15214095, 2023, 35, Downloaded from https://onlinelibrary.wiley.com/doi/10.1002/adma.202300872 by Forschungszentrum Jülich GmbH Research Center, Wiley Online Library on [10/10/2023]. See the Terms and Conditions (https://onlinelibrary.wiley.com/terms-and-conditions) on Wiley Online Library for rules of use; OA articles are governed by the applicable Creative Commons License

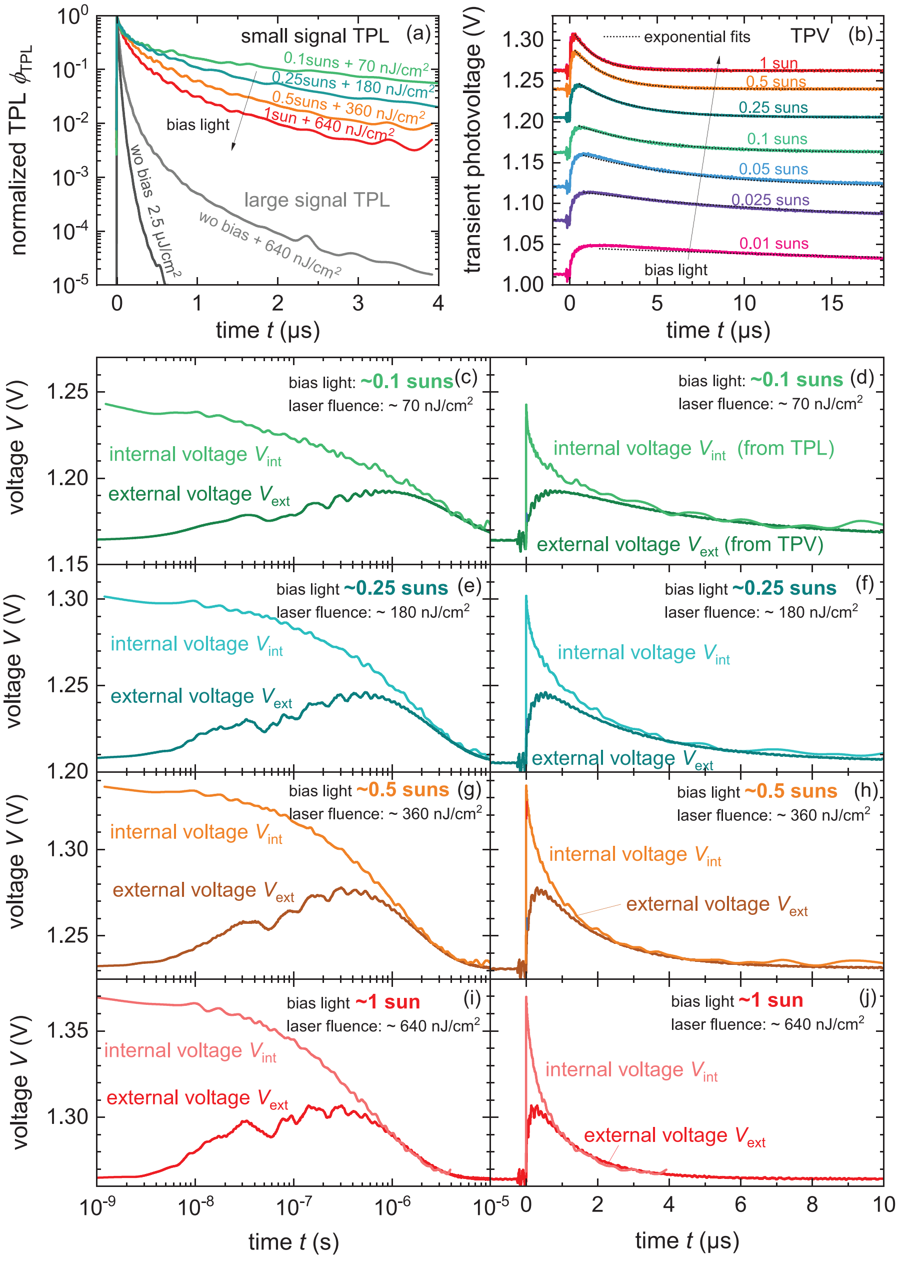

Figure 1. a,b) Experimental data of large- and small-signal transient PL measurements (a) and transient photovoltage decays (b) at different bias light intensities, measured on a MAPI solar cell. c–j) Experimental data of the internal voltage V_{int} resulting for small-signal TPL measurements and the decays of external voltage V_{ext} from TPV at different bias light intensities, measured on a MAPI solar cell. The panels on the right show the data on a logarithmic times scale, whereas the panels on the left have a linear times scale.

constants can be experimentally determined as a function of light intensity. The application of the model to experimental data allows us to derive a time constant for recombination and one for charge extraction, whereby the ratio of these two time constants is directly related to the solar cell efficiency. The results provide a significant progress relative to previous approaches[25–27,38,41,42] for the analysis of transient photovoltage data as we explicitly include the rise time[43,44] as a source of information, consider a voltage dependent resistance[45,46] of the charge-transport layers and provide a comprehensible analytical solution that can be conveniently compared with experimental data. We note further that the two-component model introduced here is generic for the rise and the decay of the photovoltage in any solar cell.

2. Experimental Data

Figure 1 shows experimental data from small-signal transient photoluminescence (TPL) and transient photovoltage (TPV) measurements, being recorded at one integrated setup illustrated

© 2023 The Authors. Advanced Materials published by Wiley-VCH GmbH

as previously discussed.[42] The internal voltage V_{int} results from small-signal TPL measurements and the corresponding external voltage decays V_{ext} from TPV at different bias light intensities. For TPL the detection was done with a gated-CCD camera as described in the method section in the Supporting Information. The internal- and external-voltage curves at four different bias levels are plotted in Figure 1c–j. The graphs on the left-hand side show the internal and external voltage curves on a logarithmic time scale, whereas the results on the left-hand side were plotted on a linear time axis. This dataset belongs to a solution-processed $\mathrm{CH_3NH_3PbI_3}$ (MAPI) solar cell, with the layer stack glass/ITO/PTAA/MAPI/PCBM/BCP/Ag, whereby PTAA is poly(triarylamine), PCBM is phenyl-C_{61}-butyric acid methyl ester, and BCP is bathocuproine. The general properties and performance of these devices were previously discussed.[19,42,47,48] In this example, the external voltage needs around several hundred nanoseconds to build up and reach its maximum voltage. Furthermore, the rise time shifts to longer times for lower steady-state excitation conditions. Note that also the decays of the internal and external voltage do not necessarily need to overlap, as the additional example of Figure S1 (Supporting Information) shows. In conclusion, these experimental results demonstrate that the exchange of the charge carriers happens with a finite speed and is possibly slow enough to interfere with the classical lifetime analysis of the TPV data. Furthermore, it becomes apparent that the internal excess voltage ΔV_{int} can be several times larger than the external excess voltage ΔV_{ext}.

3. Analysis of the Two-Component Model

The rise and decay of the externally measured photovoltage following a photoexcitation pulse implies that there are two simultaneous relaxations with opposite sign, one for the rise and the other for the decay. Thus mathematically, at least two coupled first-order differential equations with time independent coefficients are needed to describe such a behavior in general. For the transient photovoltage measurement, it is plausible that the two variables in these differential equations should be: i) the concentration of photogenerated charge carriers inside the absorber of the solar cell and ii) the externally measured photovoltage. While the concentration of charge carriers in absorber is created near instantaneously by the laser pulse, it takes some time for the charge carriers to be transported to the electrodes and thereby allow the external voltage to reach its maximum value. Thus, the photovoltage interacts with the charge carrier concentration but must be considered as an additional free variable in the system.

The first differential equation describing the kinetics of charge carrier concentration n in the absorber contains the usual terms for recombination and generation but additionally a term for the exchange current J_{exc} flowing to or from the electrodes. A positive value of J_{exc} reduces the carrier density in the absorber because carrier as extracted from the absorber to the electrode. Alternatively, if the value is negative, charge carriers injected from the electrodes flow back into the absorber layer. For a perfectly symmetric system in high-level injection, i.e., if the electron concentration n equals the hole concentration p and the external voltage V_{ext} drops to equal amounts over the electron and over the hole contact. With this the differential equation for the electron concentration reads

$$\begin{aligned}\frac{dn}{dt} &= -k_{\mathrm{rad}} n^2 - \frac{n}{\tau_{\mathrm{SRH}}^{\mathrm{eff}}} - \frac{J_{\mathrm{exc}}}{qd} + G \\ &= -k_{\mathrm{rad}} n^2 - \frac{n}{\tau_{\mathrm{SRH}}^{\mathrm{eff}}} - \frac{S_{\mathrm{exc}}}{d}\left(n - n_{\mathrm{i}} \exp\left(\frac{qV_{\mathrm{ext}}}{2kT}\right)\right) + G \qquad (1)\end{aligned}$$

where k_{rad} is the radiative recombination coefficient, $\tau_{\mathrm{SRH}}^{\mathrm{eff}}$ is the effective Shockley–Read–Hall (SRH) recombination lifetime, q is the elementary charge, d is the thickness of the absorber, and G is the generation rate. The quantity S_{exc} in the second line of Equation (1) is an exchange velocity in units of cm s^{-1}. Thus, the extraction of charge carriers from the absorber is linear in the concentration n, with S_{exc} acting as the proportionality constant, similar to a surface recombination velocity, with the only difference that the carriers do not recombine but are extracted to the contact. To satisfy the principle of detailed balance,[49] carrier extraction from the absorber to the contact and carrier injection from the contact back into the absorber must be interlinked. The way how the exchange current is represented in Equation (1) follows Ref. [50] and is also compatible with an extended equivalent circuit model for solar cells.[51] The ratio d/S_{exc} between the thickness d and the exchange velocity S_{exc} defines a time constant for the increase and decrease of the carrier densities (per unit volume, assumed constant over a thickness d) caused by the exchange current flowing to or from the electrodes.

The exchange of electrons between the absorber and the contact determines the change of the excess charge density σ_{n} per area on the n-type electrode according to

$$\frac{d\sigma_{\mathrm{n}}}{dt} = qS_{\mathrm{exc}}\left[n - n_{\mathrm{i}} \exp\left(\frac{qV_{\mathrm{ext}}}{2kT}\right)\right] \qquad (2)$$

Equation (2) implies that every electron that is extracted from the absorber contributes to the contact charge density. Likewise, every electron that is re-injected from the contact reduces the charge density. Eventually, this charge density defines the external voltage V_{n} that drops over the contact according to $V_{\mathrm{n}} = \sigma_{\mathrm{n}}/C_{\mathrm{co,n}}$where $C_{\mathrm{co,n}}$ denotes the capacitance of the n-type contact. In order to keep the model simple, we assume that the contacts are completely symmetric, i.e., we have not only the same S_{exc} for both types of contacts but the capacitance $C_{\mathrm{co,n}} = C_{\mathrm{co,p}}$ are also the same and therefore also the voltages $V_{\mathrm{n}} = V_{\mathrm{p}}$ over the electron and the hole contact. Thus, we have for the external voltage $V_{\mathrm{ext}} = V_{\mathrm{n}} + V_{\mathrm{p}} = 2V_{\mathrm{n}}$ and for the total electrical capacitance $1/C_{\mathrm{el}} = 1/C_{\mathrm{co,n}} + 1/C_{\mathrm{co,p}} = 2/C_{\mathrm{co,n}}$. From this, the time derivative of the external voltage follows as

$$\frac{dV_{\mathrm{ext}}}{dt} = \frac{qS_{\mathrm{exc}}}{C_{\mathrm{el}}}\left(n - n_{\mathrm{i}} \exp\left(\frac{qV_{\mathrm{ext}}}{2kT}\right)\right) \qquad (3)$$

Thus, Equations (1) and (3) represent the required system of two coupled differential equations. Since the variables are a carrier concentration and an electrostatic potential, Equations (1) and (3) represent a mixed system in terms of the described quantities. Therefore, one might wish to replace the carrier

© 2023 The Authors. Advanced Materials published by Wiley-VCH GmbH

15214095, 2023, 35, Downloaded from https://onlinelibrary.wiley.com/doi/10.1002/adma.202300872 by Forschungszentrum Jülich GmbH Research Center, Wiley Online Library on [10/10/2023]. See the Terms and Conditions (https://onlinelibrary.wiley.com/terms-and-conditions) on Wiley Online Library for rules of use; OA articles are governed by the applicable Creative Commons License

concentration by the splitting ΔE_{F} of the quasi-Fermi levels according to

$$n(t) = p(t) = n_{\mathrm{i}} \exp\left(\frac{\Delta E_{\mathrm{F}}(t)}{2kT}\right) = n_{\mathrm{i}} \exp\left(\frac{qV_{\mathrm{int}}(t)}{2kT}\right) \tag{4}$$

where we have replaced ΔE_{F} by qV_{int}, bearing in mind that this internal voltage V_{int} does not represent a voltage in the electrostatic sense but rather is used to conveniently relate the chemical potential of charge carriers within the device to the true, externally measurable voltage V_{ext}. With $dV_{\mathrm{int}}/dn = 2kT/(qn)$ the relation between the time derivative of V_{int} and the carrier concentration n reads

$$\begin{aligned}\frac{dV_{\mathrm{int}}}{dt} = \frac{2kT}{qn(V_{\mathrm{int}})}\Bigg[&-k_{\mathrm{rad}}n(V_{\mathrm{int}})^2 - \frac{n(V_{\mathrm{int}})}{\tau_{\mathrm{SRH}}^{\mathrm{eff}}} \\ &-\frac{S_{\mathrm{exc}}}{d}\left(n(V_{\mathrm{int}}) - n_i \exp\left(\frac{qV_{\mathrm{ext}}}{2KT}\right)\right) + G\Bigg]\end{aligned} \tag{5}$$

Now the combination of Equations (3) and (5) yields a more convenient system of two coupled differential equations describing the kinetics of two potentials. The model described so far has a clear advantage relative to our recent approach[42] as it explicitly considers differences between external voltage and internal quasi-Fermi level splitting, expressed as internal voltage. Therefore, the model can be used to simulate the rise and the decay of the photovoltage, and not only the decay.

In the following, we concentrate on the theoretical description of the small-signal response that is typically used in TPV measurements. In a large-signal analysis the response of the unbiased sample is recorded over a long period of time until the luminescence or photovoltage signal vanishes. In contrast, a small signal analysis is performed on a sample that is kept under a constant light bias condition, preferably at open circuit. Then the sample's response to a small additional light pulse is recorded. This situation allows us to linearize Equations (3) and (5) around the steady state of the bias condition, i.e., $dV_{\mathrm{int}}/dt = dV_{\mathrm{ext}}/dt = 0$ for a given $n_{\mathrm{bias}} = p_{\mathrm{bias}} = n_{\mathrm{i}}\exp(qV_{\mathrm{int}}/2k_{\mathrm{B}}T)$ and for $V_{\mathrm{int}} = V_{\mathrm{ext}}$, because the assumed open circuit condition allows neither carrier extraction nor injection. Thus, linearization of Equation (5) yields for the kinetics of small variations δV_{ext} and δV_{int} of the external and internal voltage after the light pulse

$$\begin{aligned}\frac{d}{dt}\delta V_{\mathrm{int}} &= \frac{2kT}{qn_{\mathrm{bias}}}\left[-2k_{\mathrm{rad}}n_{\mathrm{bias}} - \frac{1}{\tau_{\mathrm{SRH}}^{\mathrm{eff}}} - \frac{S_{\mathrm{exc}}}{d}\right]\frac{dn}{dV_{\mathrm{int}}}\delta V_{\mathrm{int}} \\ &\quad + \frac{2kT}{qn_{\mathrm{bias}}}\frac{S_{\mathrm{exc}}}{d}\frac{qn_{\mathrm{bias}}}{2kT}\delta V_{\mathrm{ext}} = \left[-2k_{\mathrm{rad}}n_{\mathrm{bias}} - \frac{1}{\tau_{\mathrm{SRH}}^{\mathrm{eff}}} - \frac{S_{\mathrm{exc}}}{d}\right]\delta V_{\mathrm{int}} \\ &\quad + \frac{S_{\mathrm{exc}}}{d}\delta V_{\mathrm{ext}}\end{aligned} \tag{6}$$

For the linearization of Equation (3) we obtain

$$\begin{aligned}\frac{d}{dt}\delta V_{\mathrm{ext}} &= \frac{qS_{\mathrm{exc}}}{C_{\mathrm{el}}}\frac{dn}{dV_{\mathrm{int}}}\delta V_{\mathrm{int}} - \frac{qS_{\mathrm{exc}}}{C_{\mathrm{el}}}\frac{q}{2kT}n_{\mathrm{bias}}\delta V_{\mathrm{ext}} \\ &= \frac{qS_{\mathrm{exc}}}{C_{\mathrm{el}}}\frac{q}{2kT}n_{\mathrm{bias}}\delta V_{\mathrm{int}} - \frac{qS_{\mathrm{exc}}}{C_{\mathrm{el}}}\frac{q}{2kT}n_{\mathrm{bias}}\delta V_{\mathrm{ext}}\end{aligned} \tag{7}$$

Note that in Equations (6) and (7) we have used $dn/dV_{\mathrm{int}} = dn/dV_{\mathrm{ext}} = qn_{\mathrm{bias}}/(2kT)$ for the given open circuit bias condition.

In the next step, we summarize Equations (6) and (7) into a matrix equation

$$\frac{d}{dt}\begin{pmatrix}\delta V_{\mathrm{int}} \\ \delta V_{\mathrm{ext}}\end{pmatrix} = -\begin{pmatrix}\left(\frac{1}{\tau_{\mathrm{SRH}}^{\mathrm{eff}}} + 2k_{\mathrm{rad}}n_{\mathrm{bias}} + \frac{S_{\mathrm{exc}}}{d}\right) & -\frac{S_{\mathrm{exc}}}{d} \\ -\frac{S_{\mathrm{exc}}}{d}\frac{n_{\mathrm{bias}}}{n_{\mathrm{Q}}} & \frac{S_{\mathrm{exc}}}{d}\frac{n_{\mathrm{bias}}}{n_{\mathrm{Q}}}\end{pmatrix}\begin{pmatrix}\delta V_{\mathrm{int}} \\ \delta V_{\mathrm{ext}}\end{pmatrix} \tag{8}$$

where we use the definition $n_{\mathrm{Q}} = 2C_{\mathrm{el}}kT/(q^2d)$. With the definition of the chemical capacitance of the electrons in the perovskite absorber $C_{\mu} = n_{\mathrm{bias}}q^2d/(2kT)$,[52] the ratio $n_{\mathrm{bias}}/n_{\mathrm{Q}} = C_{\mu}/C_{\mathrm{el}}$ just equals the ration between chemical and electrical capacitance.

The general solution of Equation (8) in terms of eigenvectors and eigenvalues is given by

$$\begin{pmatrix}\delta V_{\mathrm{int}} \\ \delta V_{\mathrm{ext}}\end{pmatrix}(t) = a\begin{pmatrix}h_1 \\ -1\end{pmatrix}\exp\left(-\frac{t}{\tau_{\mathrm{rise}}}\right) + b\begin{pmatrix}h_2 \\ 1\end{pmatrix}\exp\left(-\frac{t}{\tau_{\mathrm{decay}}}\right) \tag{9}$$

As the initial condition for the solution of Equation (8), we use $\delta V_{\mathrm{ext}} = 0$ and $\delta V_{\mathrm{int}} = \delta V_{\mathrm{int}}^0$, i.e., after the light pulse a certain amount of charge carriers is generated inside the absorber but the external voltage is still unaffected at time $t = 0$. From the initial values we chose the coefficient a and b such that

$$\delta V_{\mathrm{ext}}(t) = \frac{\delta V_{\mathrm{int}}^0}{h_1 + h_2}\left(\exp\left(-\frac{t}{\tau_{\mathrm{decay}}}\right) - \exp\left(-\frac{t}{\tau_{\mathrm{rise}}}\right)\right) \tag{10}$$

and

$$\delta V_{\mathrm{int}}(t) = \frac{\delta V_{\mathrm{int}}^0}{h_1 + h_2}\left(h_1\exp\left(-\frac{t}{\tau_{\mathrm{rise}}}\right) + h_2\exp\left(-\frac{t}{\tau_{\mathrm{decay}}}\right)\right) \tag{11}$$

Thus, Equation (10) describes the kinetics of the photovoltage $\delta V_{\mathrm{ext}}(t)$ that rises from zero at $t = 0$ and decays to zero toward $t \to \infty$, while Equation (11) describes the decay of the internal voltage $\delta V_{\mathrm{int}}(t)$ with two time constants. The rise and decay times τ_{rise} and τ_{decay} are the inverses of the two eigenvalues of the matrix in Equation (8), with τ_{rise} being the inverse of the larger eigenvalue such that $\delta V_{\mathrm{ext}}(t) > 0$ for all $t > 0$. The explicit calculation of the eigenvalues yields

$$\tau_{\mathrm{rise/decay}} = \frac{2}{k_1 + k_2 + k_3 \pm \sqrt{(k_1 + k_2 + k_3)^2 - 4k_1k_3}} \tag{12}$$

whereby the "+" in front of the square root is for τ_{rise} and the "−" for τ_{decay}. The amplitudes of $\delta V_{\mathrm{ext}}(t)$ and $\delta V_{\mathrm{int}}(t)$ are defined by the coefficients

$$h_{1,2} = \frac{\pm(k_1 + k_2 - k_3) + \sqrt{(k_1 + k_2 + k_3)^2 - 4k_1k_3}}{2k_3} \tag{13}$$

with $k_1 = 1/\tau_{\mathrm{SRH}}^{\mathrm{eff}} + 2k_{\mathrm{rad}}n_{\mathrm{bias}}$, $k_2 = S_{\mathrm{exc}}/d$, and $k_3 = S_{\mathrm{exc}}n_{\mathrm{bias}}/(n_{\mathrm{Q}}d)$. The "+" in Equation (13) before the round bracket is for h_1 while the "−" is for h_2. The three inverse time constants k_1, k_2, and k_3 originate from the entries of the matrix in

© 2023 The Authors. Advanced Materials published by Wiley-VCH GmbH

15214095, 2023, 35, Downloaded from https://onlinelibrary.wiley.com/doi/10.1002/adma.202300872 by Forschungszentrum Jülich GmbH Research Center, Wiley Online Library on [10/10/2023]. See the Terms and Conditions (https://onlinelibrary.wiley.com/terms-and-conditions) on Wiley Online Library for rules of use; OA articles are governed by the applicable Creative Commons License

15214095, 2023, 35, Downloaded from https://onlinelibrary.wiley.com/doi/10.1002/adma.202300872 by Forschungszentrum Jülich GmbH Research Center, Wiley Online Library on [10/10/2023]. See the Terms and Conditions (https://onlinelibrary.wiley.com/terms-and-conditions) on Wiley Online Library for rules of use; OA articles are governed by the applicable Creative Commons License

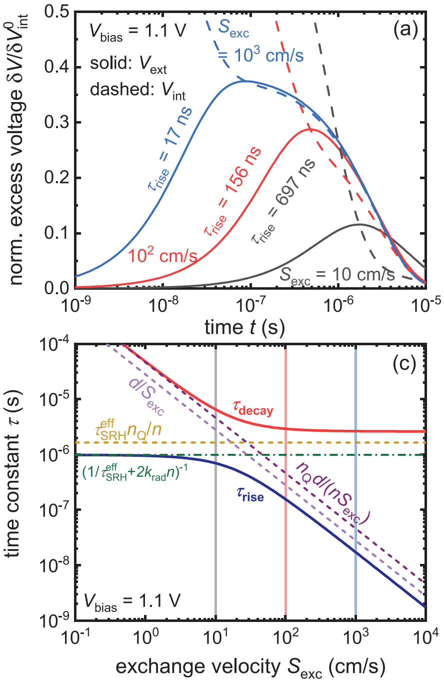

Figure 2. a,b) Analytical solutions of the normalized internal excess-voltage decay $\delta V_{int}(t)/\delta V^0_{int}$ (dashed lines) and the respective normalized external voltage $\delta V_{ext}(t)/\delta V^0_{int}$ curve (solid lines) at 1.1 V (a) and 1.25 V (b) bias voltage, calculated for three exchange velocities S_{exc}, namely 1000 cm s^{-1} (blue), 100 cm s^{-1} (red) and 10 cm s^{-1} (gray). The rise of the normalized external voltage is prolonged for smaller exchange velocities. Additional parameters used for the calculations are a SRH lifetime τ^{eff}_{SRH} = 1 µs, a radiative recombination coefficient $k_{rad} = 5 \times 10^{-11}$ cm^3 s^{-1}, an absorber-layer thickness d of 280 nm, an intrinsic carrier concentration $n_i = 8.05 \times 10^4$ cm^{-3} and a capacitance per area C_{el} = 20 nF cm^{-2}. c,d) Development of the decay time τ_{decay} and rise time τ_{rise} of the external voltage, defined by Equation (12) as a function of the exchange velocity S_{exc}. Furthermore, additional time constants related to the eigenvalues of the matrix are depicted as guide to the eye.

Equation (8), where k_1 represents the actual inverse recombination lifetime combining SRH and radiative recombination at the given working condition, and k_2 and k_3 represent the exchange rates between the absorber and the contacts.

4. Results from the Analytical Two-Component Model

Equations (10) and (11) allow us to calculate analytical solutions of the additional internal voltage $\delta V_{int}(t)$ and external voltage $\delta V_{ext}(t)$. The former would be the equivalent of a small signal transient photoluminescence curve, while the latter corresponds to a transient photovoltage signal. Examples of the respective analytical solutions of the normalized excess voltages $\delta V_{int}(t)/\delta V^0_{int}$ are shown in the upper two panels of **Figures 2** and **3**. With the help of these two Figures, we will successively discuss the influence of two important parameters on the $\delta V(t)$ curves, namely the exchange velocity S_{exc} and the electrode capacitance per area C_{el}.

Figure 2a,b visualize the analytical solutions of the matrix equation for a variation of the exchange velocity S_{exc} at two different bias levels of 1.1 V and 1.25 V. The normalized external voltage $\delta V_{ext}(t)/\delta V^0_{int}$ curves are plotted as solid lines, whereas the corresponding normalized internal voltage decays $\delta V_{int}(t)/\delta V^0_{int}$, being calculated via Equation (11), are depicted as dashed lines. For the calculation of these graphs, we used three different exchange velocities S_{exc}, a high value of 10^3 cm s^{-1} (blue), a medium value of 100 cm s^{-1} (red) and a small one of S_{exc} = 10 cm s^{-1} (gray). The exchange velocity S_{exc} depends on the properties of the charge-transport layers, such as the mobility or electric field distribution. Accordingly, the value of S_{exc} determines how quickly electrons or holes are extracted or injected through the two transport layers. The other additional parameters, being necessary to calculate the voltage curves are listed in the figure caption of Figure 2.

Our first observation is that the analytical solution of the two-component model reflects the basic trend of the internal and external voltage curves from experiment. The normalized internal excess voltage $\delta V_{int}(t)/\delta V^0_{int}$ is highest at the very beginning and continues to decrease over time until it reaches the initial bias voltage. In contrast, the response of the normalized external excess voltage $\delta V_{ext}(t)/\delta V^0_{int}$ to the small-signal excitation is delayed. It increases slowly over time, reaches its maximum and only then begins to decay. Thus, this model is able to reproduce the general features of the TPV transient. Furthermore, the variation of the exchange velocity S_{exc}, shows that rise of the additional external voltage is prolonged for smaller exchange velocities and the maximum of the curves shifts to longer times. This trend occurs at both shown bias levels. The associated rise times τ_{rise}, calculated via Equation (9), are indicated next to the curves and quantify the described trend. The decay of $\delta V_{ext}(t)/\delta V^0_{int}$, on the other hand, is affected differently by the variation of exchange velocity for the two bias levels. In panel 2(a) at the lower injection level of 1.1 V, a change in S_{exc} also affects the decay of the curves, whereas at

© 2023 The Authors. Advanced Materials published by Wiley-VCH GmbH

15214095, 2023, 35, Downloaded from https://onlinelibrary.wiley.com/doi/10.1002/adma.202300872 by Forschungszentrum Jülich GmbH Research Center, Wiley Online Library on [10/10/2023]. See the Terms and Conditions (https://onlinelibrary.wiley.com/terms-and-conditions) on Wiley Online Library for rules of use; OA articles are governed by the applicable Creative Commons License

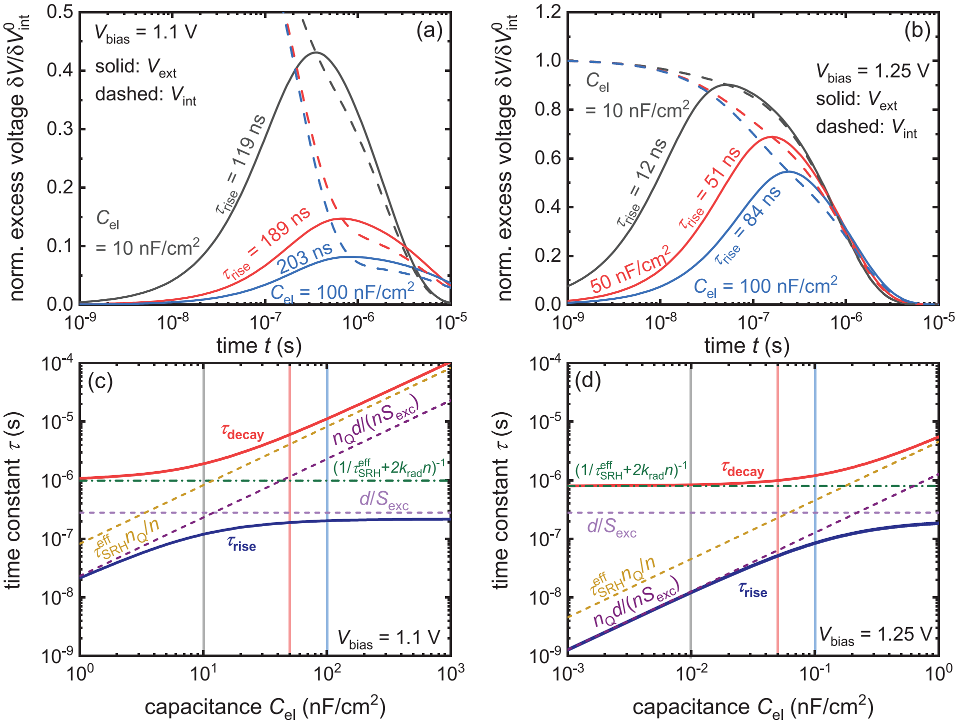

Figure 3. a,b) Analytical solutions of the normalized internal excess-voltage decay $\delta V_{int}(t)/\delta V^0_{int}$ (dashed line) and the respective normalized external excess-voltage curve of $\delta V_{ext}(t)/\delta V^0_{int}$ (solid line) at 1.1 V (a) and 1.25 V (b) bias voltage, calculated for three different values of the electrode capacitance per area C_{el}. The capacitance per area C_{el} is varied between 20 nF cm^{-2} (gray), 50 nF cm^{-2} (red), and 100 nF cm^{-2} (blue). Besides a constant exchange velocity of S_{exc} = 100 cm s^{-1}, other simulation parameters are equal to Figure 2. c,d) Rise time τ_{rise} and decay time τ_{decay} from Equation (12) as a function of the electrode capacitance per area C_{el} for the two different bias levels. Furthermore, additional time constants related to the eigenvalues of the matrix are shown as guide to the eye.

1.25 V in panel 2(b) all three decays of the normalized external voltage $\delta V_{ext}(t)/\delta V^0_{int}$ overlap. Note that the decay time τ_{decay}, as well as the rise time τ_{rise} are injection-level dependent and therefore differ between Figure 2a,b. At the higher bias voltage, the respective rise time τ_{rise} is shorter and increases by an order of magnitude when the exchange velocity decreases by an order of magnitude, thus follows a power law function while this inverse proportionality disappears in case of the lower bias voltage. To better understand the behavior, Figure 2c,d directly depict the rise time τ_{rise} and decay time τ_{decay} as a function of the exchange velocity S_{exc} for the two different bias levels. Furthermore, additional time constants related to the eigenvalues of the matrix and the inverse coefficients $1/k_1$, $1/k_2$, and $1/k_3$ are shown as guide to the eye. In addition, the parameter sets of the three different examples from the top figures are marked as well by thin, vertical lines.

The rise-time curve τ_{rise}, shown as thick, blue line, can be divided into two sections. For low exchange velocities S_{exc} the rise time is constant and determined by the recombination lifetime (or inverse time constant k_1), namely $\tau_R = (1/\tau^{eff}_{SRH} + 2k_{rad}n_{bias})^{-1} = 1/k_1$ (green, dashed line). If the exchange is fast in comparison to recombination the rise time gets shorter with increasing exchange velocity S_{exc}. At the lower injection level of 1.1 V and high exchange velocities, the rise time depends on the ratio of d/S_{exc} (lilac, dashed line). Thus, in this case τ_{rise} is dominated by the resistance of charge extraction through the charge-transfer layers and the chemical capacitance of the perovskite layer, which represent an RC-time constant. At high bias voltages (in our example: 1.25 V) as shown in Figure 2d, the rise time τ_{rise} follows the RC-time constant $n_Qd/(S_{exc}n_{bias})$ which is formed by the resistance of charge extraction multiplied with the electrode capacitance of the solar cell. The decay time τ_{decay}, being calculated by using Equation (12), is shown as thick, red line. In the regime where charge transfer is fast in comparison with recombination, the decay time of the external voltage is constant and does not depend on S_{exc}. Depending on the bias level the corresponding saturation value of τ_{decay} is set either by the time constant $\tau^{eff}_{SRH}n_Q/n_{bias}$ of the electrode being discharged via recombination in the perovskite or—at high bias levels—by recombination $\tau_R = (1/\tau^{eff}_{SRH} + 2k_{rad}n_{bias})^{-1}$. If the exchange velocity is small, charge transfer also affects the decay time τ_{decay} of the normalized external voltage $\delta V_{ext}(t)/\delta V$, which then approaches $n_Qd/(S_{exc}n_{bias})$ (purple, dashed line). This discussion shows that depending on the injection level and parameter set, different time constants determine both the rise and fall of the small-signal TPV curve.

Figure 3a,b show the normalized internal excess voltage $\delta V_{int}(t)/\delta V^0_{int}$ (dashed line) and the respective external voltage $\delta V_{ext}(t)/\delta V^0_{int}$ (solid line) calculated from Equation (10) for two different bias levels. In addition, the lower two bottom panels (c)

© 2023 The Authors. Advanced Materials published by Wiley-VCH GmbH

and (d) again plot the time constants of the rise and decay, but this time as a function of capacitance C_{el}. Higher capacitances imply that more charge carriers have to be transferred from the perovskite to the electrodes to accommodate a given change in external voltage. Thus, a higher value of C_{el} slows down both the rise and fall of the normalized internal and external voltage curves, reduces the height of the $\delta V_{\text{ext}}(t)/\delta V_{\text{int}}^0$ peak and affects the shape of the curves. Moreover, the rise- and decay-time curves again consist of two regions for both shown bias voltages. In one region τ_{decay} and τ_{rise} are constant, while they are following a power law and increase for higher C_{el} in the other one. The decay time τ_{decay} does not depend on C_{el} if the time constant of electrode discharging is small in comparison to the recombination lifetime τ_{R}. In this regime, which almost disappears in case of lower bias voltage of 1.1 V, τ_{decay} is limited by the green, dashed line. In the second regime, the decay time increases with higher electrode capacitance C_{el} and follows the yellow, dashed line of $\tau_{\text{SRH}}^{\text{eff}} n_{\text{Q}}/n_{\text{bias}}$. The rise time τ_{rise} is proportional to $n_{\text{Q}} d/(S_{\text{exc}} n_{\text{bias}})$ and therefore increases with higher capacitance until this time constant gets larger than the RC-element formed by the resistance of charge extraction and the chemical capacitance of the absorber layer. The RC-limitation that sets the saturation value of the rise time is not universal and depends on the relations of the respective time constants to each other.

We observed in Figure 2 and Figure 3 that in addition to parameters such as C_{el}, S_{exc}, k_{rad}, and $\tau_{\text{SRH}}^{\text{eff}}$ also the bias voltage affects the time constants for rise and decay. Thus, it has been common practice in particular in organic photovoltaics, to plot TPV-derived decay time as a function of either carrier density or open-circuit voltage.[26,53,54] **Figure 4** shows the rise time τ_{rise} and decay time τ_{decay} as a function of the bias open-circuit voltage V_{oc}. The three Figure 4a-c on the left-hand side show the time constants versus V_{oc} for three voltage-independent values of S_{exc}, (1000 cm s^{-1}, 100 cm s^{-1}, 10 cm s^{-1}). The decay time τ_{decay}, (red line) shows three distinct regions, the capacitively limited region at low V_{oc}, the SRH dominated region at intermediate V_{oc} and the region limited by radiative recombination at high V_{oc}.[42] These three regions correspond to the three regions discussed in our previous work.[19,42] The rise time τ_{rise} (blue line) shows two distinct regions. At low bias voltages the τ_{rise} is constant, while at high bias voltages it continuously decreases with $\tau_{\text{rise}} \sim 1/n_{\text{bias}}$. What changes significantly for the three different exchange velocities is the position and distance of the two time-constant curves relative to each other. Moreover, depending on the exchange velocity, different RC-time constants dominate the regimes and saturation values of τ_{rise} and τ_{decay}. The left-hand column of Figure 4 serves primarily to explain fundamentally how the different terms in the matrix in Equation (8) affect the rise and decay times and how as a function of voltage, different terms in matrix become dominant. However, panels (a) to (c) treat S_{exc} as a voltage-independent constant.

As the speed of charge injection and extraction via the transport layers depends on the electric field, it is, however, realistic to expect S_{exc} to depend on bias voltage. At short circuit, a good analytical approximation for S_{exc} is given by $S_{\text{exc}} = \mu \overline{F_{\text{CTL}}}/(1-\exp(-\Delta V_{\text{el}}/kT))$,[45,55] where μ is the mobility of electrons and holes in both transport layers, $\overline{F_{\text{CTL}}}$ is the average electric field and ΔV_{el} is the electrostatic potential drop over the charge transport layers (i.e., electric field times thickness). Thus, the exchange velocity S_{exc} is related to the product of mobility and electric field in the charge transport layers, which would be the drift velocity of charge carriers in that layer. We have recently discussed the merits of this equation for explaining charge collection losses at short circuit.[55] However, toward opencircuit, when the electric field gets smaller and is affected by space charge of free carriers, the equation becomes inaccurate.

Thus, we calculate the voltage dependence of S_{exc} from numerical drift-diffusion simulations of device current–voltage curves as described in Section III.f (Supporting Information). These drift-diffusion simulations have the advantage relative to the analytical equation discussed above that they are able to consider the space charge of free charge carriers and are therefore not limited to bias conditions close to short circuit. Figure 4d–f now mirror the panels (a) to (c) but for the case of voltage-dependent values of S_{exc}. The panels (d) to (f) differ in the values of the electron and hole mobilities in the transport layers ($\mu = 10^{-2}$ cm^2 V^{-1}s^{-1} in (d) to $\mu = 10^{-4}$ cm^2 V^{-1}s^{-1} in (f)) that we assumed in the drift-diffusion simulations (see **Figure 5**a for the actual values). The mobilities are chosen such that they lead to values of S_{exc} that are on the same order of magnitude as the values in the adjacent panel on the left. On the right-hand column of Figure 4, those dashed lines that contain S_{exc} will now have a voltage dependence. Note that we only labeled the dashed lines that do change in order to highlight them.

For the case of Figure 4d,e, τ_{decay} only depends on terms ($\tau_{\text{SRH}}^{\text{eff}} n_{\text{Q}}/n_{\text{bias}}$ at low V_{oc} and $\tau_{\text{R}} = (1/\tau_{\text{SRH}}^{\text{eff}} + 2k_{\text{rad}} n_{\text{bias}})^{-1}$ at high V_{oc}) that do not contain S_{exc}. Thus, τ_{decay} is basically the same as in the panels on the left. In Figure 4f, the purple dashed line ($n_{\text{Q}} d/(S_{\text{exc}} n_{\text{bias}})$) becomes relevant at high and hence there are deviations for τ_{decay}. In contrast to τ_{decay}, the voltage dependence of τ_{rise} changes considerably in all three panels. Relative to the left-hand columns with constant S_{exc},the rise time now depends less strongly on bias voltage and shows a relatively flat plateau at intermediate voltages.

Figure 4 shows that rise and decay times are dominated by several different terms depending on the relative values of the different time constants. The high complexity of Equation (12) however does not give direct access to the important time constants. To understand and identify the most important time constants for rise and decay it is therefore useful to simplify Equation (12) further.

A Taylor series expansion of Equation (12) allows us to mathematically approximate the decay time τ_{decay} and simplify it to the point where the behavior that is described above can be read directly from the equation (for details see Section III.d, Supporting Information). In this approximation, the decay time results from

$$\tau_{\text{decay}} \approx \frac{k_1+k_2+k_3}{k_1 k_3} = \left(\frac{1}{\tau_{\text{R}}} + \frac{S_{\text{exc}}}{d} + \frac{S_{\text{exc}} n_{\text{bias}}}{n_{\text{Q}} d}\right) \Big/ \left(\frac{1}{\tau_{\text{R}}} \frac{S_{\text{exc}} n_{\text{bias}}}{n_{\text{Q}} d}\right) = \frac{n_{\text{Q}} d}{S_{\text{exc}} n_{\text{bias}}} + \frac{\tau_{\text{R}} n_{\text{Q}}}{n_{\text{bias}}} + \tau_{\text{R}} \tag{14}$$

which corresponds to a series connection of the recombination lifetime and both RC-time constants from electrode discharging

© 2023 The Authors. Advanced Materials published by Wiley-VCH GmbH

15214095, 2023, 35, Downloaded from https://onlinelibrary.wiley.com/doi/10.1002/adma.202300872 by Forschungszentrum Jülich GmbH Research Center, Wiley Online Library on [10/10/2023]. See the Terms and Conditions (https://onlinelibrary.wiley.com/terms-and-conditions) on Wiley Online Library for rules of use; OA articles are governed by the applicable Creative Commons License

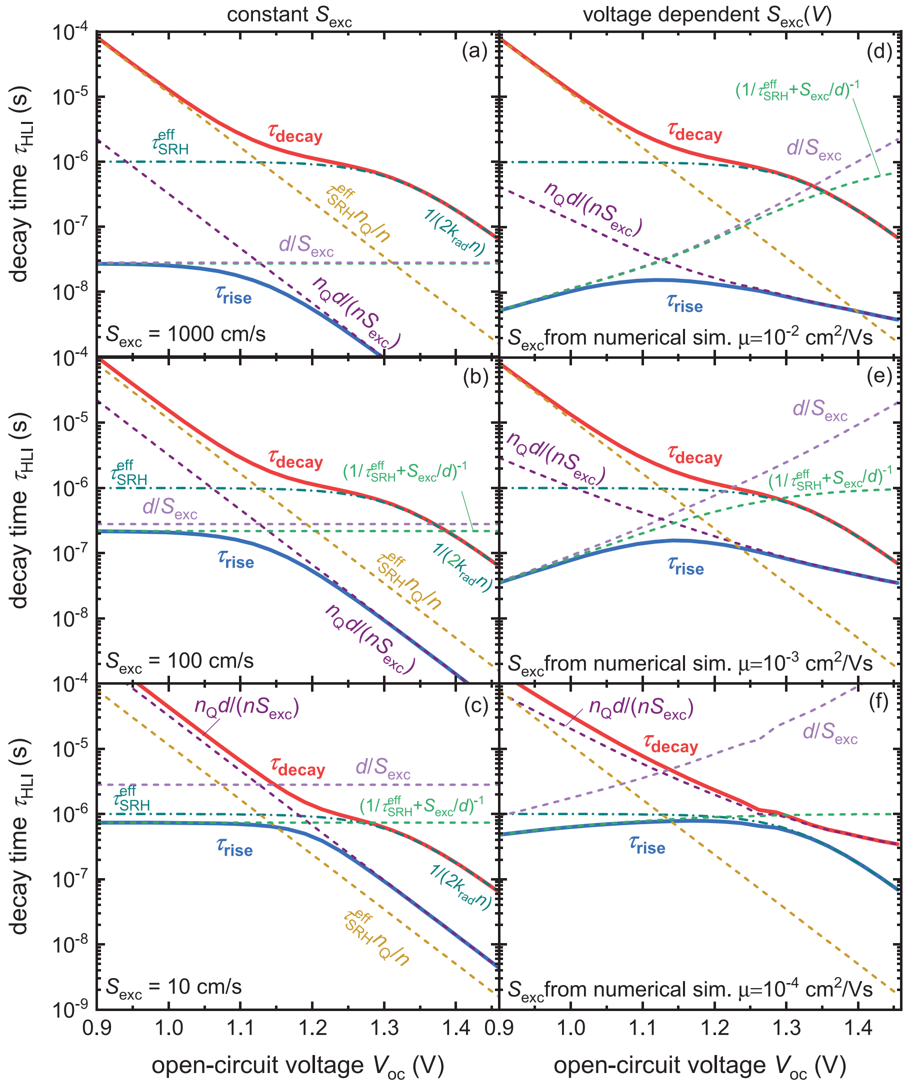

Figure 4. Decay time τ_{decay} (red) and rise time τ_{rise} (blue) as a function of the open-circuit voltage V_{oc}, calculated using Equation (12). In addition, the inverse coefficients $1/k_2 = d/S_{\text{exc}}$ and $1/k_3 = n_{\text{Q}}d/(S_{\text{exc}}n_{\text{bias}})$ are plotted, as well as additional important time constants, like $\tau_{\text{SRH}}^{\text{eff}}n_{\text{Q}}/n_{\text{bias}}$ which is related to electrode discharging. The figures in the left column show the analytical results using a constant exchange velocity S_{exc} of 10^3 cm s^{-1} (a), 100 cm s^{-1} (b), and 10 cm s^{-1} (c). In contrast (d), (e), and (f) on the right-hand side show the decay time τ_{decay} and rise time τ_{rise} for three different voltage-dependent exchange velocities S_{exc}.

and charge transfer. In the limiting case, where the exchange velocity is fast enough ($\tau_{\text{SRH}}^{\text{eff}} > d/S_{\text{exc}}$), Equation (14) can be simplified even further, resulting in

$$\tau_{\text{decay}} \approx \tau_{\text{R}}\left(1+\frac{n_{\text{Q}}}{n_{\text{bias}}}\right) = \frac{n_{\text{Q}}/n_{\text{bias}}+1}{2k_{\text{rad}}n_{\text{bias}}+1/\tau_{\text{SRH}}^{\text{eff}}} \tag{15}$$

and thereby matches Equation (12) of our previous publication.[42] Using a similar mathematical approach, also allows us to derive an approximation for the rise time

$$\tau_{\text{rise}} \approx (k_1+k_2+k_3)^{-1} = \left(\frac{1}{\tau_{\text{R}}}+\frac{S_{\text{exc}}}{d}+\frac{S_{\text{exc}}n_{\text{bias}}}{n_{\text{Q}}d}\right)^{-1} \tag{16}$$

Basically, this rise-time approximation is a parallel connection of the recombination lifetime τ_{R}, the RC-time constant d/S_{exc} given by the resistance of charge transfer multiplied with the chemical capacitance of the perovskite, and $dn_{\text{Q}}/(S_{\text{exc}}n_{\text{bias}})$, being the RC-time constant of charge-transfer resistance and electrode capacitance. If the condition $\tau_{\text{R}} > d/S_{\text{exc}}$ holds, Equation (16) can be simplified even further, resulting in

$$\tau_{\text{rise}} \approx \frac{d}{S_{\text{exc}}\left(1+\frac{n_{\text{bias}}}{n_{\text{Q}}}\right)} \tag{17}$$

which allows us to calculate S_{exc} from τ_{rise} and vice versa. Note that Equations (15) and (16) provide relatively simple approximations for the rise and decay time, each of which include n_{Q} and therefore the influence of the electrode capacitance. The

© 2023 The Authors. Advanced Materials published by Wiley-VCH GmbH

15214095, 2023, 35, Downloaded from https://onlinelibrary.wiley.com/doi/10.1002/adma.202300872 by Forschungszentrum Jülich GmbH Research Center, Wiley Online Library on [10/10/2023]. See the Terms and Conditions (https://onlinelibrary.wiley.com/terms-and-conditions) on Wiley Online Library for rules of use; OA articles are governed by the applicable Creative Commons License

15214095, 2023, 35, Downloaded from https://onlinelibrary.wiley.com/doi/10.1002/adma.202300872 by Forschungszentrum Jülich GmbH Research Center, Wiley Online Library on [10/10/2023]. See the Terms and Conditions (https://onlinelibrary.wiley.com/terms-and-conditions) on Wiley Online Library for rules of use; OA articles are governed by the applicable Creative Commons License

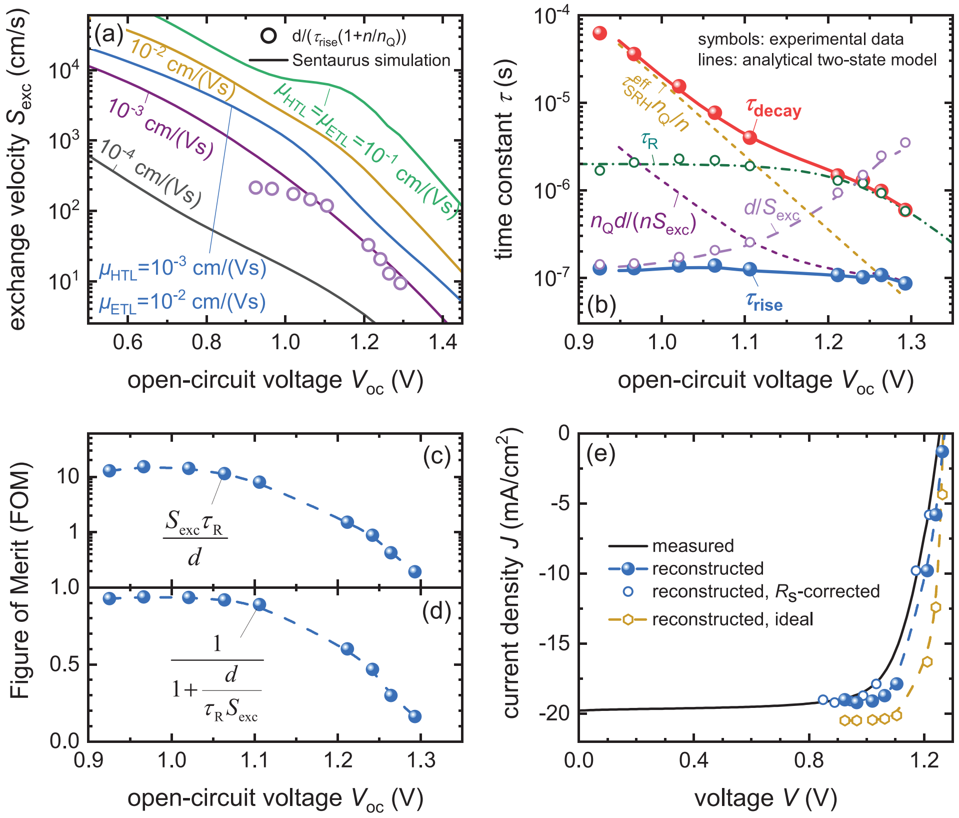

Figure 5. a) Exchange velocity S_{exc} extracted from steady-state drift–diffusion simulations of *JV*-curves, being conducted assuming various charge-carrier mobilities. Moreover, the exchange velocity S_{exc} calculated from the experimental TPV data via $S_{exc} = d/(\tau_{rise}(1 + n_{bias}/n_Q))$ is shown by the dashed symbols. b) Experimental data of the decay time τ_{decay} (red symbols) and rise time τ_{rise} (blue symbols) from TPV as a function of the open-circuit voltage V_{oc}. In addition, the analytical two-component model is fitted to experimental data. The results are shown by the lines. c,d) Figures of merit for the rate of extraction versus recombination. Panel (c) shows the ratio of the time constants. d) The prefactor in Equation (18) that quantifies the effect of a finite efficiency of extraction on the *JV* curve. e) Measured and reconstructed current–voltage characteristic of the MAPI solar cell. In (e), we assumed a generation rate $G = 4.57 \times 10^{21}$ cm^{-3} s^{-1} and for the blue open circles a series resistance $R_s = 4\ \Omega$ cm^2.

electrode capacitance has a strong impact on transient experiments performed on complete solar cells but has no direct impact on the steady-state functionality of the device. Thus, we will now investigate, how we can extract the performance limiting contributions to the rise and decay time from the capacitive contributions.

5. Application of the Analytical Two-Component Model to Experimental TPV Data

Figure 5a shows simulated values of S_{exc} resulting from different numerical drift-diffusion simulations (lines) where the mobility of electrons and holes in the charge transport layers was varied. This data is compared to values of S_{exc} resulting from the application of Equation (17) to the experimental data on a MAPI solar cell shown in Figure 5b. The experimental data shows that the recombination lifetime τ_R is approximately one order of magnitude higher than τ_{rise}, which implies that Equations (15) and (17) are both good approximations for this particular device.

As shown in the Section III.g (Supporting Information) and based on the rationale derived,[56] it is possible to use the ratio of the two time constants τ_R and d/S_{exc} to estimate the effect of slow charge extraction on the current–voltage curve and thereby performance of a solar cell. The steady-state equivalent of our two-component model allows us to calculate the current–voltage curve via

$$
\begin{aligned}
J &= qd\,(R - G)\\
&= qd\left(\frac{1}{1 + d/\left(S_{exc}\tau_R\right)}\right)\left[\frac{n_0}{\tau_R}\left(\exp\left(\frac{qV_{ext}}{2kT}\right) - 1\right) - G\right]
\end{aligned}
\tag{18}
$$

If the product $\tau_R S_{exc} >> d$, charge extraction is efficient, and Equation (18) predicts that the *JV*-curve only depends on recombination and generation (square bracket) but not on the efficiency of charge extraction (round bracket). If however $\tau_R S_{exc} \approx d$, the term in the round bracket becomes ½ and the current density is reduced by 50%. Thus, a low value of S_{exc} will reduce J_{sc} by the factor $(1 + d/(S_{exc}\tau_R))^{-1}$. A voltage dependence of this factor can then also reduce the fill factor (FF). In contrast, as open circuit is not affected by charge extraction, the open-circuit voltage remains independent of S_{exc}.

In order to quantify the efficiency of charge extraction, we have two possibilities. Option (1) is to plot the ratio of the two time constants, i.e., $\tau_R S_{exc}/d$, which is a quantity that should be

© 2023 The Authors. Advanced Materials published by Wiley-VCH GmbH

significantly larger than unity to ensure efficient collection. Alternatively, we can directly compute the factor $(1 + d/(S_{\text{exc}}\tau_{\text{R}}))^{-1}$ which is a quantity lower than one that defines the charge collection efficiency. Both figures of merit (FOMs) are shown in Figure 5c,d using the experimental data for the rise and decay time shown in Figure 5b. Here, the first figure of merit follows from

$$\text{FOM}_1 = \frac{S_{\text{exc}}\tau_{\text{R}}}{d} = \frac{\tau_{\text{decay}}}{\tau_{\text{rise}}} \frac{n_{\text{Q}} n_{\text{bias}}}{\left(n_{\text{Q}} + n_{\text{bias}}\right)^2} \tag{19}$$

while the second one can be obtained via

$$\text{FOM}_2 = \frac{1}{1 + \frac{d}{S_{\text{exc}}\tau_{\text{R}}}} = \frac{1}{1 + \frac{\tau_{\text{rise}}}{\tau_{\text{decay}}} \frac{\left(n_{\text{Q}}+n_{\text{bias}}\right)^2}{n_{\text{Q}} n_{\text{bias}}}} \tag{20}$$

Both FOMs are relatively constant between 0.9 and 1.1 V, where $\text{FOM}_1 \approx 10$ implying that extraction is significantly faster than recombination. Toward higher voltages, FOM_1 significantly reduces and quickly falls below unity. As can be seen in Figure 5b this drop is mostly due to d/S_{exc} getting significantly longer toward higher voltages. We assume that this is due to the fact that at voltages above 1.2 V likely no significant electric field is left in the transport layers. Potentially, there are even extraction barriers implying that electrons and holes would have to diffuse against the electric field to be extracted. Figure 5e illustrates the impact of the FOMs on the current–voltage curve. The solid line shows the experimentally measured current–voltage curve of the MAPI solar cell whose TPV data is shown in Figure 5b. The yellow circles show the JV-curve according to Equation (18) but assuming $S_{\text{exc}} \to \infty$. The blue spheres show the current–voltage curve according to Equation (18) with FOM_2 according to Figure 5d. We note that the JV curve shows a slightly reduced J_{sc} and FF. The change in J_{sc} is due to a $\text{FOM}_1 \approx 10$ leading to a $\text{FOM}_2 \approx 0.9$, implying a still quite significant loss in J_{sc} of just less than 10%. The FF is only moderately affected as FOM_2 is relatively voltage independent up to ≈1.1 V. The real JV-curve obviously suffers from additional losses not included in FOM_2. We assume that these additional losses are ohmic series resistance losses, e.g. due to lateral transport in the transparent conductive oxide. As ohmic losses due to lateral transport would not be included in S_{exc}, it is plausible that the blue spheres do not reproduce the JV-curve. We added an ohmic series resistance ($R_{\text{s}} = 4\ \Omega\ \text{cm}^2$) to this curve and obtain the open circles, which approximate the experimental JV-curve well.

Thus, we conclude that the FOMs are consistent with the JV-curve but would require additional information to predict the JV-curve. We also show that due to the rather low voltage dependence of S_{exc} up to the maximum power point, extraction losses are mostly affecting the J_{sc} and to a lesser degree the FF. This also implies that the FF is most likely more affected by ohmic series resistances than by the non-ohmic charge transport through ETL and HTL. This observation is consistent with other experimental findings on charge extraction such as the weak voltage dependence of steady-state photoluminescence between short circuit and the maximum-power point in perovskite solar cells.[16,48]

6. Discussion and Limitations of the Proposed Approach

Extracting parameters for extraction and recombination separately from the rise and decay of the photovoltage offers a variety of possibilities for research on halide perovskite solar cells. In particular, the approach allows us to distinguish losses due to short lifetimes at open circuit from losses due to inefficient transport of charge carriers out of the device. Thus, the impact of controlled variations of contact layer properties on recombination and extraction can be studied separately. This could in turn help to identify strength and weaknesses of employed transport layers. Eventually, with the help of Equation (18), the impact of τ_{R} and S_{exc} on the JV curve and the photovoltaic performance can be quantified and compared to the device data. With the help of this comparison, purely resistive effects can be identified and discriminated from effects due to low mobilities in intrinsic contact layers as shown in Figure 5e.

However, the approach also has some limitations. The complexity of the model is significantly smaller than that of a full drift-diffusion simulation with ions that could be considered the benchmark for device simulations in halide perovskites.[57,58] While the simplifications are an intentional feature of the model aiming to cut to the core of the problem, they imply that there is no 1:1 relationship between the parameters τ_{R} and S_{exc} and the material parameters of the solar cell. The recombination lifetime τ_{R} can be understood as representing all recombination processes including those at the interface between absorber and ETL or HTL. Thus, from the knowledge of just τ_{R} as a function of V_{oc}, it would not be possible to discriminate between interface and bulk recombination and in most cases sample type variations as described in refs. [12,15,19,59,60] are needed. However, it is possible to distinguish between recombination processes that are linear in n and those that are higher order in n (such as radiative recombination). The approach to create a 2 × 2 matrix to treat external and internal voltage relies on the contacts and charge transport layers to be either very symmetric (e.g., similarly thick and similar mobility) or very unsymmetric (as done, e.g., in the steady-state model discussed[56]). What is not possible with the model is to accurately treat an intermediate situation where both transport layers contribute significantly to the extraction losses but have very different properties that cannot be described by one variable S_{exc}. While it might be possible to create models with larger matrices, simple and comprehensible analytical expressions for the eigenvalues will only exist for 2 × 2 matrices. Thus, the key advantage of the model to provide a simple analytical explanation for rise and decay times would be lost. Furthermore, the impact of ions is treated quite generically in the present paper by assuming that ions screen the electric field in the absorber thereby allowing us to treat the absorber as a field free region with an average Fermi level splitting that is representative of the whole volume of the absorber.[45,55,61] We have experimental evidence to assume that this is a good approximation for the samples under investigation[48] but this may of course be a problematic approximation for other samples and materials. Especially in materials with lower mobilities, the depth dependence of the Fermi level splitting inside the absorber might become a dominant factor in understanding the TPV rise and decay.[38]

© 2023 The Authors. Advanced Materials published by Wiley-VCH GmbH

15214095, 2023, 35, Downloaded from https://onlinelibrary.wiley.com/doi/10.1002/adma.202300872 by Forschungszentrum Jülich GmbH Research Center, Wiley Online Library on [10/10/2023]. See the Terms and Conditions (https://onlinelibrary.wiley.com/terms-and-conditions) on Wiley Online Library for rules of use; OA articles are governed by the applicable Creative Commons License

7. Conclusions

A significant shortcoming of previous approaches to analyze small signal transient photovoltage data was that they were generally focused on obtaining only the decay time constant. While it was possible to determine rise times, there was no model to relate the rise times to devise functionality. Here, we introduce a model for charge recombination and extraction that can be linearized and solved analytically. The solutions for the rise and decay time of the transient photovoltage follow from the inverse eigenvalues of a matrix and can be related to physical mechanisms such as extraction, recombination and capacitive charging and discharging of the electrodes. We apply the model to experimental data and identify the physical mechanisms that determine the rise and decay times at different bias conditions. From the absolute value, their bias dependence and ratio of the rise and decay times, we can clearly distinguish the time constants of recombination and extraction from time constants related to capacitive effects that are irrelevant for steady-state device performance. By correcting the rise and decay times for the influence of the electrode capacitance, we obtain figures of merit for charge extraction that connect the data obtained from the transient with the current–voltage curves and thereby the performance of the device. We observe that the rise and decay times predict losses in J_{sc} of about 10% as well as minor losses in FF. The general concept of the matrix model will be applicable to a variety of small-signal transient and frequency-domain methods that are frequently used to analyze the electronic properties of halide perovskite solar cells.[29,31,32]

Supporting Information

Supporting Information is available from the Wiley Online Library or from the author.

Acknowledgements

The authors acknowledge support from the Helmholtz Association via the project PEROSEED and via the project-oriented funding (POF IV). The authors also acknowledge funding from the German Research Foundation (DFG) for the project CREATIVE within the SPP "Perovskite Semiconductors: From Fundamental Properties to Devices" (SPP 2196). Open access publication funded by the DFG – 491111487.

Open access funding enabled and organized by Projekt DEAL.

Conflict of Interest

The authors declare no conflict of interest.

Data Availability Statement

The data that support the findings of this study are available from the corresponding author upon reasonable request.

Keywords

capacitive discharge, charge-carrier lifetime, decay time, photovoltaics, time-resolved photoluminescence

Received: January 29, 2023
Revised: April 16, 2023
Published online: July 19, 2023

---

[1] J. Jeong, M. Kim, J. Seo, H. Lu, P. Ahlawat, A. Mishra, Y. Yang, M. A. Hope, F. T. Eickemeyer, M. Kim, Y. J. Yoon, I. W. Choi, B. P. Darwich, S. J. Choi, Y. Jo, J. H. Lee, B. Walker, S. M. Zakeeruddin, L. Emsley, U. Rothlisberger, A. Hagfeldt, D. S. Kim, M. Grätzel, J. Y. Kim, *Nature* **2021**, *592*, 381.
[2] J. J. Yoo, G. Seo, M. R. Chua, T. G. Park, Y. Lu, F. Rotermund, Y.-K. Kim, C. S. Moon, N. J. Jeon, J.-P. Correa-Baena, V. Bulović, S. S. Shin, M. G. Bawendi, J. Seo, *Nature* **2021**, *590*, 587.
[3] O. Almora, D. Baran, G. C. Bazan, C. I. Cabrera, S. Erten-Ela, K. Forberich, F. Guo, J. Hauch, A. W. Y. Ho-Baillie, T. J. Jacobsson, R. A. J. Janssen, T. Kirchartz, N. Kopidakis, M. A. Loi, R. R. Lunt, X. Mathew, M. D. McGehee, J. Min, D. B. Mitzi, M. K. Nazeeruddin, J. Nelson, A. F. Nogueira, U. W. Paetzold, B. P. Rand, U. Rau, H. J. Snaith, E. Unger, L. Vaillant-Roca, C. Yang, H.-L. Yip, et al., *Adv. Energy Mater.* **2023**, *13*, 2203313.
[4] M. Kim, J. Jeong, H. Lu, T. K. Lee, F. T. Eickemeyer, Y. Liu, I. W. Choi, S. J. Choi, Y. Jo, H.-B. Kim, S.-I. Mo, Y.-K. Kim, H. Lee, N. G. An, S. Cho, W. R. Tress, S. M. Zakeeruddin, A. Hagfeldt, J. Y. Kim, M. Grätzel, D. S. Kim, *Science* **2022**, *375*, 302.
[5] Q. Jiang, J. Tong, Y. Xian, R. A. Kerner, S. P. Dunfield, C. Xiao, R. A. Scheidt, D. Kuciauskas, X. Wang, M. P. Hautzinger, R. Tirawat, M. C. Beard, D. P. Fenning, J. J. Berry, B. W. Larson, Y. Yan, K. Zhu, *Nature* **2022**, *611*, 278.
[6] Z. Li, B. Li, X. Wu, S. A. Sheppard, S. Zhang, D. Gao, N. J. Long, Z. Zhu, *Science* **2022**, *376*, 416.
[7] K. Yoshikawa, H. Kawasaki, W. Yoshida, T. Irie, K. Konishi, K. Nakano, T. Uto, D. Adachi, M. Kanematsu, H. Uzu, K. Yamamoto, *Nat. Energy* **2017**, *2*, 17032.
[8] K. Yoshikawa, W. Yoshida, T. Irie, H. Kawasaki, K. Konishi, H. Ishibashi, T. Asatani, D. Adachi, M. Kanematsu, H. Uzu, K. Yamamoto, *Sol. Energy Mater. Sol. Cells* **2017**, *173*, 37.
[9] C. Ballif, F.-J. Haug, M. Boccard, P. J. Verlinden, G. Hahn, *Nat. Rev. Mater.* **2022**, *7*, 597.
[10] Y. Rong, Y. Hu, A. Mei, H. Tan, M. I. Saidaminov, S. I. Seok, M. D. McGehee, E. H. Sargent, H. Han, *Science* **2018**, *361*, eaat8235.
[11] D. Zhang, D. Li, Y. Hu, A. Mei, H. Han, *Commun. Mater.* **2022**, *3*, 58.
[12] M. Stolterfoht, M. Grischek, P. Caprioglio, C. M. Wolff, E. Gutierrez-Partida, F. Peña-Camargo, D. Rothhardt, S. Zhang, M. Raoufi, J. Wolansky, M. Abdi-Jalebi, S. D. Stranks, S. Albrecht, T. Kirchartz, D. Neher, *Adv. Mater.* **2020**, *32*, 2000080.
[13] L. Krückemeier, U. Rau, M. Stolterfoht, T. Kirchartz, *Adv. Energy Mater.* **2020**, *10*, 1902573.
[14] S. Cacovich, G. Vidon, M. Degani, M. Legrand, L. Gouda, J.-B. Puel, Y. Vaynzof, J.-F. Guillemoles, D. Ory, G. Grancini, *Nat. Commun.* **2022**, *13*, 2868.
[15] M. Stolterfoht, P. Caprioglio, C. M. Wolff, J. A. Marquez, J. Nordmann, S. Zhang, D. Rothhardt, U. Hörmann, Y. Amir, A. Redinger, L. Kegelmann, F. Zu, S. Albrecht, N. Koch, T. Kirchartz, M. Saliba, T. Unold, D. Neher, *Energy Environ. Sci.* **2019**, *12*, 2778.
[16] M. Stolterfoht, V. M. Le Corre, M. Feuerstein, P. Caprioglio, L. J. A. Koster, D. Neher, *ACS Energy Lett.* **2019**, *4*, 2887.
[17] W. Tress, M. Yavari, K. Domanski, P. Yadav, B. Niesen, J. P. Correa Baena, A. Hagfeldt, M. Graetzel, *Energy Environ. Sci.* **2018**, *11*, 151.
[18] P. Caprioglio, C. M. Wolff, O. J. Sandberg, A. Armin, B. Rech, S. Albrecht, D. Neher, M. Stolterfoht, *Adv. Energy Mater.* **2020**, *10*, 2000502.

© 2023 The Authors. Advanced Materials published by Wiley-VCH GmbH

15214095, 2023, 35, Downloaded from https://onlinelibrary.wiley.com/doi/10.1002/adma.202300872 by Forschungszentrum Jülich GmbH Research Center, Wiley Online Library on [10/10/2023]. See the Terms and Conditions (https://onlinelibrary.wiley.com/terms-and-conditions) on Wiley Online Library for rules of use; OA articles are governed by the applicable Creative Commons License

[19] L. Krückemeier, B. Krogmeier, Z. Liu, U. Rau, T. Kirchartz, *Adv. Energy Mater.* **2021**, *11*, 2003489.
[20] E. M. Hutter, T. Kirchartz, B. Ehrler, D. Cahen, E. v. Hauff, *Appl. Phys. Lett.* **2020**, *116*, 100501.
[21] T. Kirchartz, J. A. Márquez, M. Stolterfoht, T. Unold, *Adv. Energy Mater.* **2020**, *10*, 1904134.
[22] F. Staub, H. Hempel, J. C. Hebig, J. Mock, U. W. Paetzold, U. Rau, T. Unold, T. Kirchartz, *Phys. Rev. Appl.* **2016**, *6*, 044017.
[23] S. Feldmann, S. Macpherson, S. P. Senanayak, M. Abdi-Jalebi, J. P. H. Rivett, G. Nan, G. D. Tainter, T. A. S. Doherty, K. Frohna, E. Ringe, R. H. Friend, H. Sirringhaus, M. Saliba, D. Beljonne, S. D. Stranks, F. Deschler, *Nat. Photonics* **2020**, *14*, 123.
[24] J. M. Richter, M. Abdi-Jalebi, A. Sadhanala, M. Tabachnyk, J. P. H. Rivett, L. M. Pazos-Outon, K. C. Gödel, M. Price, F. Deschler, R. H. Friend, *Nat. Commun.* **2016**, *7*, 13941.
[25] D. Kiermasch, L. Gil-Escrig, A. Baumann, H. J. Bolink, V. Dyakonov, K. Tvingstedt, *J. Mater. Chem. A* **2019**, *7*, 14712.
[26] D. Kiermasch, A. Baumann, M. Fischer, V. Dyakonov, K. Tvingstedt, *Energy Environ. Sci.* **2018**, *11*, 629.
[27] Z. S. Wang, F. Ebadi, B. Carlsen, W. C. H. Choy, W. Tress, *Small Methods* **2020**, *4*, 2000290.
[28] A. O. Alvarez, S. Ravishankar, F. Fabregat-Santiago, *Small Methods* **2021**, *5*, 2100661.
[29] S. Ravishankar, A. Riquelme, S. K. Sarkar, M. Garcia-Batlle, G. Garcia-Belmonte, J. Bisquert, *J. Phys. Chem. C* **2019**, *123*, 24995.
[30] J. Bisquert, M. Janssen, *J. Phys. Chem. Lett.* **2021**, *12*, 7964.
[31] J. Bisquert, *J. Phys. Chem. Lett.* **2022**, *13*, 7320.
[32] A. Guerrero, J. Bisquert, G. Garcia-Belmonte, *Chem. Rev.* **2021**, *121*, 14430.
[33] A. Kiligaridis, P. A. Frantsuzov, A. Yangui, S. Seth, J. Li, Q. An, Y. Vaynzof, I. G. Scheblykin, *Nat. Commun.* **2021**, *12*, 3329.
[34] F. Peña-Camargo, J. Thiesbrummel, H. Hempel, A. Musiienko, V. M. L. Corre, J. Diekmann, J. Warby, T. Unold, F. Lang, D. Neher, M. Stolterfoht, *Appl. Phys. Rev.* **2022**, *9*, 021409.
[35] B. Krogmeier, F. Staub, D. Grabowski, U. Rau, T. Kirchartz, *Sustainable Energy Fuels* **2018**, *2*, 1027.
[36] J. Haddad, B. Krogmeier, B. Klingebiel, L. Krückemeier, S. Melhem, Z. Liu, J. Hüpkes, S. Mathur, T. Kirchartz, *Adv. Mater. Interfaces* **2020**, *7*, 2000366.
[37] C. Fai, A. J. C. Ladd, C. J. Hages, *Joule* **2022**, *6*, 2585.
[38] M. Azzouzi, P. Calado, A. M. Telford, F. Eisner, X. Hou, T. Kirchartz, P. R. F. Barnes, J. Nelson, *Sol. RRL* **2020**, *4*, 1900581.
[39] C. Cho, S. Feldmann, K. M. Yeom, Y.-W. Jang, S. Kahmann, J.-Y. Huang, T. C. J. Yang, *Nat. Mater.* **2022**, *21*, 1388.
[40] G. Vidon, S. Cacovich, M. Legrand, A. Yaiche, D. Ory, D. Suchet, J.-B. Puel, J.-F. Guillemoles, *Phys. Rev. Appl.* **2021**, *16*, 044058.
[41] S. Wheeler, D. Bryant, J. Troughton, T. Kirchartz, T. Watson, J. Nelson, J. R. Durrant, *J. Phys. Chem. C* **2017**, *121*, 13496.
[42] L. Krückemeier, Z. Liu, B. Krogmeier, U. Rau, T. Kirchartz, *Adv. Energy Mater.* **2021**, *11*, 2102290.
[43] B. C. O'Regan, K. Bakker, J. Kroeze, H. Smit, P. Sommeling, J. R. Durrant, *J. Phys. Chem. B* **2006**, *110*, 17155.
[44] P. R. F. Barnes, K. Miettunen, X. Li, A. Y. Anderson, T. Bessho, M. Gratzel, B. C. O'Regan, *Adv Mater* **2012**, *25*, 1881.
[45] O. J. Sandberg, J. Kurpiers, M. Stolterfoht, D. Neher, P. Meredith, S. Shoaee, A. Armin, *Adv. Mater. Interfaces* **2020**, *7*, 2000041.
[46] S. Ravishankar, Z. Liu, U. Rau, T. Kirchartz, *PRX Energy* **2022**, *1*, 013003.
[47] Z. Liu, L. Krückemeier, B. Krogmeier, B. Klingebiel, J. A. Marquez, S. Levcenko, S. Öz, S. Mathur, U. Rau, T. Unold, T. Kirchartz, *ACS Energy Lett.* **2019**, *4*, 110.
[48] D. Grabowski, Z. Liu, G. Schöpe, U. Rau, T. Kirchartz, *Sol. RRL* **2022**, *6*, 2200507.
[49] P. W. Bridgman, *Phys. Rev.* **1928**, *31*, 101.
[50] U. Rau, *IEEE J. Photovoltaics* **2012**, *2*, 169.
[51] O. Breitenstein, *IEEE J. Photovoltaics* **2014**, *4*, 899.
[52] J. Bisquert, *Phys. Chem. Chem. Phys.* **2003**, *5*, 5360.
[53] D. Credgington, J. R. Durrant, *J. Phys. Chem. Lett.* **2012**, *3*, 1465.
[54] J. Wu, H. Cha, T. Du, Y. Dong, W. Xu, C.-T. Lin, J. R. Durrant, *Adv. Mater.* **2022**, *34*, 2101833.
[55] S. Akel, A. Kulkarni, U. Rau, T. Kirchartz, *PRX Energy* **2023**, *2*, 013004.
[56] U. Rau, V. Huhn, B. E. Pieters, *Phys. Rev. Appl.* **2020**, *14*, 014046.
[57] N. Tessler, Y. Vaynzof, *ACS Energy Lett.* **2020**, *5*, 1260.
[58] P. Calado, A. M. Telford, D. Bryant, X. Li, J. Nelson, B. C. O'Regan, P. R. F. Barnes, *Nat. Commun.* **2016**, *7*, 13831.
[59] V. Sarritzu, N. Sestu, D. Marongiu, X. Chang, S. Masi, A. Rizzo, S. Colella, F. Quochi, M. Saba, A. Mura, G. Bongiovanni, *Sci. Rep.* **2017**, *7*, 44629.
[60] M. Stolterfoht, C. M. Wolff, J. A. Márquez, S. Zhang, C. J. Hages, D. Rothhardt, S. Albrecht, P. L. Burn, P. Meredith, T. Unold, D. Neher, *Nat. Energy* **2018**, *3*, 847.
[61] J. Hüpkes, U. Rau, T. Kirchartz, *Sol. RRL* **2022**, *6*, 2100720.

© 2023 The Authors. Advanced Materials published by Wiley-VCH GmbH

15214095, 2023, 35, Downloaded from https://onlinelibrary.wiley.com/doi/10.1002/adma.202300872 by Forschungszentrum Jülich GmbH Research Center, Wiley Online Library on [10/10/2023]. See the Terms and Conditions (https://onlinelibrary.wiley.com/terms-and-conditions) on Wiley Online Library for rules of use; OA articles are governed by the applicable Creative Commons License